A NUMERICAL PARAMETRIC STUDY OF THE EFFECTIVENESS OF THE 4-SIDED IMPACT ROLLER

Yue Chen[1], Mark B. Jaksa[2], Brendan T. Scott[2] and Yien-Lik Kuo[2]
[1] University of New South Wales, Canberra, [2] University of Adelaide

https://doi.org/10.56295/AGJ5822

ABSTRACT

Rolling dynamic compaction (RDC) is a specific type of dynamic compaction, which involves towing a heavy non-circular module at a relatively constant speed. This paper investigates the effects of module mass, operating speed and varying ground conditions on the effectiveness of the 4-sided impact roller using a developed finite element method (FEM)-discrete element method (DEM) model. Numerical results were analysed from four aspects, namely the energy imparted to the ground, soil velocity vectors, module imprint lengths and soil displacements at different depths. It is found that, a heavier module mass induces greater ground improvement in terms of both energy delivered to the soil per impact and the magnitude of soil displacements. The energy imparted to the underlying soil by the module increases with greater operating speed. The rotational dynamics of the module also change with increasing operating speed, whereby the impacts are delivered by the faces of the module at typical operating speeds; however, at faster speeds the impacts are delivered towards the corners of the module and the behaviour is less reproducible. The modelling showed that soil with a higher initial Young's modulus and a higher internal angle of friction decreases the magnitude of soil displacements, which confirms that the impact roller is less able to significantly improve soils that are stiff or have a high initial shear strength.

1 INTRODUCTION

With the growing demand for infrastructure development, there is an increasing need to construct on sites, which were previously considered to be difficult or unsuitable. In order to facilitate construction, soils at marginal sites typically require improvement. Compaction is the most frequently used method to improve the ground mechanically, as it is both efficient and cost-effective. Rolling dynamic compaction (RDC), is a specific type of dynamic compaction, which involves towing a heavy non-circular module at relatively constant speed. As it is towed, the module rotates and falls to impact the ground dynamically, whereby both potential and kinetic energies are imparted to the underlying soil during this process. RDC has been applied successfully in various ground improvement contexts, such as, civil and mining projects, land reclamation projects and highway rehabilitation (Avalle and Carter, 2005; Avalle and McKenzie, 2005; Bouazza and Avalle, 2006). Although RDC has been employed in several projects, as reported by Scott and Jaksa (2008), there are situations, after compaction, in which the soil did not meet the expected requirements. A key reason why it is not more widely used, is that the use of RDC is based, to a large extent, on previous experience in similar ground conditions (Scott and Jaksa, 2008). Therefore, there is a need to investigate factors that affect the performance of RDC and then provide practical recommendations for applications of RDC.

The effectiveness of RDC is mainly affected by three aspects: the ground conditions, RDC operation and the characteristics of RDC module. Scott et al. (2019) reported that the effective depth of influence of RDC is affected by the soil conditions and the operating speed. A greater effective depth of influence is achieved in coarse soil and at a faster operating speed. Scott et al. (2020) examined the influence of RDC operating speed (5–15 km/h) using buried earth pressure cells (EPCs) in field tests. It was found that the recorded peak pressure increased as the operating speed grew from 5 to 12 km/h, and the peak pressure reduced at operating speed greater than 12 km/h. They also reported that a greater energy was imparted by RDC at faster operating speeds. Previous studies on the effectiveness of RDC were mainly conducted in the field and over several years (Avalle and Carter, 2005; Jaksa et al., 2012; Scott and Jaksa, 2014; Scott et al., 2016; Jaksa et al., 2019). Whilst there are many benefits of conducting field tests, they are expensive because they require a significant amount of time and effort to prepare and carry out the field tests. Measurement and instrumentation is usually complex and provides limited insights into the performance of RDC. In addition, homogeneous soils need to be employed in the field tests in order to quantify the effect of a single factor on the ground improvement results and also to ensure the accuracy of test results. The influence of the operation of RDC and the characteristics of RDC module, such as the operating speed, the number of RDC passes, and the weight and the shape of RDC module are easier to assess since these are factors that can be controlled by the RDC operator. However, the effects of site conditions on the performance of

RDC are difficult to be assessed in field tests since ground conditions, such as the type, the initial dry density and the particle size range of the soil are site-specific, complex and difficult to control in field tests.

Since conducting field tests suffers from several disadvantages, as mentioned above, an alternate approach, which is capable of assessing factors that influence the effectiveness of RDC, is highly desirable. In recent years, numerical modelling has been successfully adopted by several researchers to investigate the performance of RDC (Kuo et al., 2013; Bradley et al., 2019; Chen et al., 2021). Based on their studies, it can be concluded that the developed numerical models provide reasonable predictions of ground improvement due to RDC and the effectiveness of RDC is able to be quantified based on the numerical results. In addition, parameters that affect the soil properties can be varied and controlled with relative ease in a numerical model, which facilitates enhanced understanding of the effects of these parameters on the ground improvement results.

By the use of a numerical model developed by Chen et al. (2021), this study seeks to explore the influence of module mass, operating speed and varying ground conditions on the performance of a 4-sided impact roller. The numerical model is used to quantify the energy imparted to the ground, soil velocity vectors, module imprint lengths and soil displacements at different depths, and these are used to study the effectiveness of RDC with different module weights, at various operating speeds and in different ground conditions, as is discussed below.

2 NUMERICAL MODEL

The numerical RDC scale model adopted in this study was developed by Chen et al. (2021) using the LS-DYNA computer application (LSTC 2018). The model consists of a simplified 1:13 scaled roller module, a chamber filled with soil particles and two rigid frames at each end of the chamber, as shown in Figure 1. The scaled roller module, the chamber and two frames are simulated using the finite element method (FEM), while the soil particles are simulated using the discrete element method (DEM). The chamber and two frames are modelled as rigid materials and fixed at their initial locations in the model, with no displacement or deformation during the roller compaction process. The scaled module is a 1:13 scale replica of the Broons' 4-sided impact roller and the properties of the scaled module are calculated according to scaling laws proposed by Altaee and Fellenius (1994) [Equations (1)-(5)]. The roller module is modelled as a rigid body with no deformation during compaction, since the roller is relatively rigid compared with the stiffness of the soil (Kuo et al., 2013; Bradley et al., 2019). The size of the chamber is 600 × 280 × 125 mm (length × width × height) to accommodate the 1:13 scaled module with dimensions of 115 × 100 × 115 mm (length × width × height). The actual soil particles are simulated as rigid spheres with soft contacts, which implies that the particles are permitted to overlap at the contacts. The contact forces between particles are evaluated using a contact model. In Chen et al. (2021), the linear contact model was adopted, since it is simple, reliable and efficient. The linear contact model contains two linear elastic springs in the normal and shear directions with constant normal (k_n) and shear (k_s) stiffnesses, respectively; two viscous damping dashpots in the normal and shear directions with normal (β_n) and shear (β_s) damping ratios, respectively; and a frictional slip in the shear direction with a coefficient of friction, μ. Input parameters of the linear contact model were calibrated through numerical triaxial tests to ensure the numerical particles exhibit similar macroscopic behaviour to the actual soil particles. In addition, the rotation of the numerical particles was prohibited to simulate the irregular shape of soil particles and increase the macroscopic shear strength of the numerical particles (Calvetti et al., 2003; Calvetti et al., 2004; Gabrieli et al., 2009). In the numerical model, soil particles were generated to fill an enclosed box and then fell into the chamber under gravity from a relatively constant height.

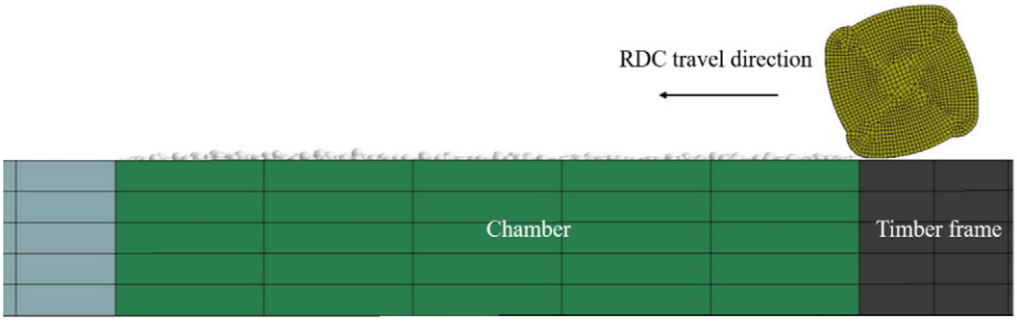

Figure 1: Numerical model setup.

The developed numerical scale model was validated against results obtained from field tests conducted by Scott et al. (2016). The numerical results were upscaled based on the scaling laws developed by Altaee and Fellenius (1994) [Equations (6)-(8)]. The upscaled numerical results were then compared against field data obtained from the same soil properties using a full-size RDC module. It was concluded that, the upscaled numerical results were in good agreement with the field data and the numerical scale model was demonstrated to be able to simulate reliably the behaviour of the full-size RDC model. Consequently, the numerical scale model can be used to provide practical recommendations for the application of the full-size RDC module.

$$\frac{L_m}{L_p} = n \tag{1}$$

$$\frac{V_m}{V_p} = n^3 \tag{2}$$

$$\frac{M_m}{M_p} = n^3 \tag{3}$$

$$\frac{T_m}{T_p} = 1 \tag{4}$$

$$\frac{S_m}{S_p} = n \tag{5}$$

$$\frac{D_m}{D_p} = n \cdot \frac{\frac{\Delta e_m}{1+e_{0m}}}{\frac{\Delta e_p}{1+e_{0p}}} \tag{6}$$

$$\frac{\sigma_m}{\sigma_p} = \exp\left(\frac{e_{0p}-e_{0m}}{\lambda}\right) \tag{7}$$

$$\frac{E_m}{E_p} = \exp\left(\frac{e_{0p}-e_{0m}}{\lambda}\right) \times n^3 \tag{8}$$

where L is the characteristic length; V and M are the volume and mass of the roller module, respectively; T is the operating time; S is the operating speed; D is the vertical displacement; σ is the imposed stress; E is the energy imparted by the module; e_0 is the initial void ratio; Δe is the change in void ratio; λ is the slope of the critical state line in the e – log σ plane; n is the geometric scale ratio (1/13); and the subscripts m and p denote the scale model and prototype (i.e. the full-size module), respectively.

The soil used in this study is the same as that adopted by Chen et al. (2021), therefore, the DEM input parameters calibrated by Chen et al. (2021) are used. In addition, similar to Chen et al. (2021), in the numerical RDC tests, due to the computational and time constraints, the particles are upscaled to be 3.5 times greater than the particle size used in the calibration triaxial tests. The calibrated DEM input parameters were then upscaled using the mass scaling law developed by Gabrieli et al. (2009). The upscaled DEM input parameters are shown in Table 1, and these are the input parameters used in numerical RDC tests in this study.

Table 1: DEM input parameters used in numerical RDC tests.

Parameter	Value
Particle density (kg/m^3)	2,620
Particle diameter (mm)	3.5–10.5
Coefficient of friction (μ)	0.25
Normal and shear stiffnesses (k_n and k_s) (N/m)	2.275 ×10^6
Normal and shear damping ratios (β_n and β_s)	0.1

Two different weights (3.64 and 5.46 kg) of 4-sided scale modules are studied, which represent the 8- and 12-tonne impact rollers (Broons BH-1300 and BH-1300 HD), respectively. Operating speeds of 192, 214, 235, 256, 278, 299 and 321 mm/s, corresponding to the full-size operating speeds of 9, 10, 11, 12, 13, 14 and 15 km/h, respectively, are evaluated. The matrix of numerical simulations, which investigates the effects of module weight and operating speed, is shown in Table 2. Each simulation consists of 5 module passes. As with Chen et al. (2021), the numerical simulations are performed using a University of Adelaide's supercomputer (2 × Intel Xeon Gold

6248 Processor @2.4 GHz) using the ANSYS (LS-DYNA) software. Due to ANSYS license constraints, 12 CPU cores were used for these simulations. Typically, each simulation took approximately 5 days to run. The influence of varying the ground conditions on RDC performance is presented later in the paper.

Table 2: Simulation matrix.

Simulation no.	Scaled module weight (kg)	Full-size module weight (tonne)	Scaled module operating speed (mm/s)	Full-size module operating speed (km/h)
1	5.46	12	235	11
2	3.64	8	235	11
3	3.64	8	192	9
4	3.64	8	214	10
5	3.64	8	256	12
6	3.64	8	278	13
7	3.64	8	299	14
8	3.64	8	321	15

3 MODULE WEIGHT

Simulations 1 and 2 are conducted to assess the effect of module weight on the ground improvement results. The energy imparted to the ground by a single module impact is an important indicator of the effectiveness of RDC (Scott and Jaksa, 2008; Li et al., 2020). LS-DYNA provides the energy imparted by the module during compaction process based on the motion of the module. The total energy of the roller, which consists of kinetic and potential energies, can be calculated using LS-DYNA at each time step. The kinetic energy of the roller is obtained based on the horizontal, vertical and rotational speeds of the roller. The potential energy of the roller is predicted by tracking the vertical displacements of the roller in LS-DYNA. Therefore, the energy delivered to the ground per roller impact is obtained using the total energy of the roller before the impact minus the total energy of the roller after the impact. In the numerical model, horizontal speed of the roller is defined based on the full-size roller traveling speed, and the vertical speed is calculated by the model according to the defined horizontal speed, the soil properties and the undulating surface left by previous module impacts. It is worth restating that the numerical simulations are conducted using the 1:13 RDC scaled module and the numerical results need to be upscaled to replicate the field data. Therefore, the energy scaling factor [Equation (8)] is used to upscale the numerical results. The initial void ratio of the soil in the numerical model is approximately 0.764, and the average initial void ratio of the soil in the field tests was reported as 0.52 (Scott et al. 2016). Consistent with Chen et al. (2021), $\lambda = 0.11$ is adopted in this study. The energy results are interrogated from several module impacts from Simulations 1 and 2 and then upscaled using the energy scaling factor [Equation (8)]. As a consequence, it is determined, with 95% confidence, that the 8- and 12-tonne modules deliver approximately 24 ± 3 and 35 ± 4 kJ to the soil per impact, respectively, for an operating speed of 11 km/h.

Velocity vectors of soil particles directly reflect the soil's response to the influence of RDC. Figures 2 and 3 display velocity vectors of soil particles as a result of RDC for both the 8- and 12-tonne modules. In general, it can be seen that the overall soil displacement pattern induced by the 8-tonne module is similar to that of the 12-tonne module. By comparing the two, the heavier module (i.e. 12-tonne) induces larger velocity vectors at the its highest location and after the module's impact, which is evidenced by Figures 2b and 3b. In addition, the 12-tonne module has a greater influence region, which means more soil particles are affected by the heavier module, as one might expect. This is again shown by the velocity vectors observed at deeper depths and greater lengths from the contact point between the module and the soil in Figures 2b and 3b.

As indicated by the soil movements in Figures 2 and 3, the energy imparted to soil as a consequence of RDC dissipates in all directions (i.e. spread from top to bottom and from the centre of impact to both sides). This phenomenon was also reported by Li et al. (2020), who stated that the energy induced by a 3-sided RDC module dissipates in all directions based on particle movements captured by a high-speed camera.

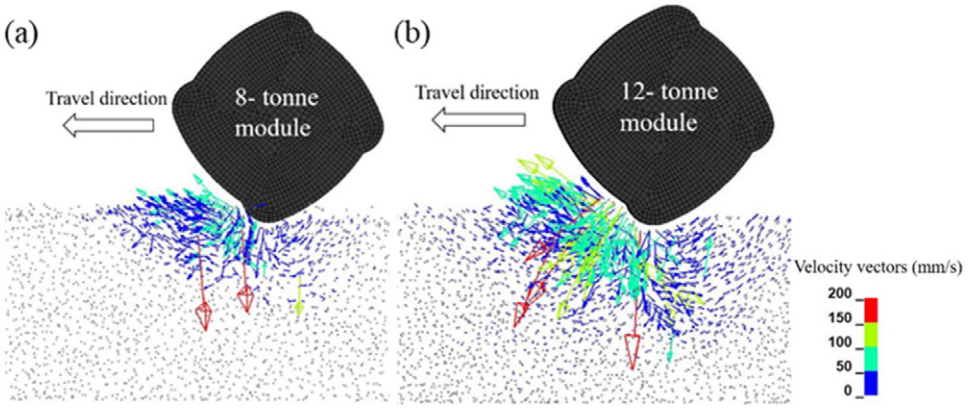

Figure 2: Velocity vectors of soil particles at the module's highest location: (a) 8-tonne module, (b) 12-tonne module.

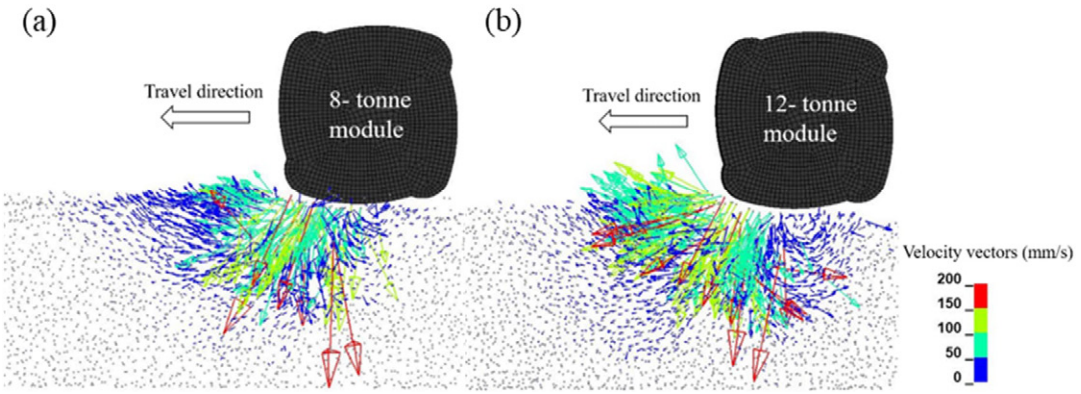

Figure 3: Velocity vectors of soil particles just after the module's impact: (a) 8-tonne module, (b) 12-tonne module.

In general, from the numerical results, it can be concluded that, the 12-tonne module achieves greater efficacy in compacting the ground when compared with the 8-tonne module, in terms of imparting a greater amount of energy to the ground and inducing larger soil displacements. However, in practice, the decision between using an 8- or 12-tonne module is often made based on several other factors. For example, the heavier module induces greater ground vibrations, which may result in the need for a greater buffer zone to settlement sensitive infrastructure to minimise the effects of vibrations. A field trial is recommended before the actual application to assess the effects of ground vibrations to nearby structures. In addition, the heavier module is less mobile than the lighter one, which adds to the cost of transporting and operating the module. The heavier module also imposes greater surface pressures and may be a more marginal option at traversing the ground surface at sites containing loose sands, or soft clays, or where the water table may be close to the surface. Therefore, the choice between the 8- and 12-tonne modules should be made by giving due consideration to all of these factors.

4 OPERATING SPEED

Simulations 3-8 were conducted and the results of Simulations 2-8 are analysed to investigate the influence of operating speed on the performance of RDC. The range of operating speeds used in this study was selected based on the typical operating speed range of the 4-sided roller (9–12 km/h) and the conclusions drawn from the experimental tests performed by Chen et al. (2022). Chen et al. (2022) conducted experimental tests to examine the effects of operating speeds on soil displacements induced by the roller. Four different operating speeds, which correspond to 10, 12, 14, and 16 km/h, were investigated in their study. It was found that, the 16 km/h operating speed provided fewer soil displacements compared with those induced by the roller operated at 14 km/h. Therefore, the operating speed range was selected as 9–15 km/h in this study. The energy delivered to the ground is again adopted as a measure of the effectiveness of RDC. As stated in the previous section, the energy imparted to the

soil from LS-DYNA is interrogated from several module impacts and then upscaled. Table 3 shows the summary of the energy imparted per module impact with varying operating speed. In general, the energy increases with faster operating speeds. Bradley et al. (2019) quantified the energy delivered by RDC by analysing the motion of the 4-sided module from a field test using high-speed photography. The authors concluded that the energy imparted by the module per impact was reported as 23 ± 4 kJ at an operating speed of 10 km/h, which is consistent with the energy results obtained in the present study. In addition, Table 4 presents the energy imparted to the ground per module impact for operating speeds between 9–12 km/h reported by Scott et al. (2020). From Table 4, it again shows that the imparted energy increases with greater operating speed. It can be further seen that the energy results obtained by Scott et al. (2020) are slightly greater than those from the results of the numerical simulations in the present study. The reason is that energies delivered to the soil reported by Scott et al. (2020) are the theoretically possible maximum values, and these values may not be imparted to the ground at each module impact, since the ground conditions vary at each site and this affects the full delivery of potential energy.

Table 3: Energy imparted by the module at different operating speeds with 95% confidence.

Operating speed (km/h)	9	10	11	12	13	14	15
Energy absorbed by the ground per module impact (kJ)	21 ± 2	22 ± 2	24 ± 3	26 ± 3	30 ± 3	32 ± 4	33 ± 4

Table 4: Energy imparted by the module at operating speeds between 9 to 12 km/h (Scott et al., 2020).

Operating speed (km/h)	9	10	11	12
Energy imparted per module impact (kJ)	22	25	27	30

Operating speed not only affects the amount of energy delivered to the underlying soil, but also influences the way that the energy is imparted to the ground. Clifford (1980) stated that the 4-sided roller can deliver sufficient energy to the ground, per impact blow, when the operating speed is within the range of 9–12 km/h. At operating speeds slower than this range, may result in sliding of the module on the ground, since the roller has insufficient momentum to keep the module rotating. Again, according to Clifford (1980), when the operating speed is greater than this range, the module starts to skip on the ground and the energy is delivered by the corners rather than the faces of the module. Avalle et al. (2009) and Scott et al. (2020) reported the same phenomenon. Scott et al. (2020) further confirmed these findings by measuring the spacing between contact imprints left on the ground after each impact. The authors stated that, when the operating speed is within the recommended range, the energy is delivered by the face of the module, the imprints left on the ground are relatively uniform and the spacings between them are approximately equal to the length of the module's face (i.e. 1,450 mm). At higher speeds than those recommended, the module tends to skip on the ground from corner to corner, the imprints become non-uniform, and the spacings between them varies within a wide range and they are generally greater than the module face length. Therefore, the module imprint lengths on the ground are measured in the numerical simulations and upscaled using Equation (1) in order to compare them with those of Scott et al. (2020).

As illustrated in Figure 4, the module imprint length shows an increasing trend as the operating speed grows. As indicated, the solid line represents the length of the module's face (1,450 mm). The cross symbols in Figure 4 represent the average of the imprint lengths obtained from around ten module impacts from the numerical simulations. It can be seen that the average of the module imprint lengths obtained from speeds of 9–11 km/h are smaller than the module face length due to insufficient kinetic energy of the roller module. On the other hand, the average module imprint length is greater than the module face length at an operating speed of 15 km/h, due to the erratic movements of the module at higher speeds. For speeds between 12 to 14 km/h, the average module imprint lengths are close to the module face length. The trend of the changes of module imprint length with respect to the operating speed is similar to that reported by Scott et al. (2020). However, Scott et al. (2020) found that the imprint length is greater than the module face length at speeds greater than 13 km/h. This discrepancy is likely due to the following two reasons. Firstly, the soil properties in the numerical model and the field tests, such as soil grading, particle sizes and initial relative density, are not identical, and the soil was simulated as spherical particles in the numerical models, while the soil used in the field tests was angular in shape. Furthermore, Kim (2011) reported

that the roller skipped on the ground with stiff soils at a speed of 10 km/h, which indicates that the operating speed also depends on the soil conditions. Secondly, the double-spring-linkage system which is incorporated in the full-sized module may increase the likelihood of the module skipping behaviour. On the other hand, the discrepancy confirms the observation reported by Scott et al. (2020) that the recommended operating speed should be varied based on the site-specific ground conditions.

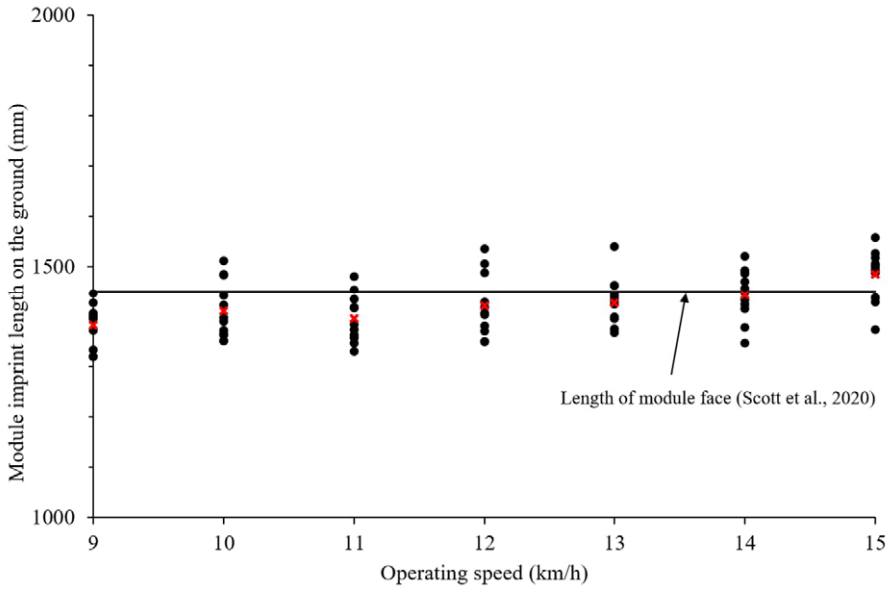

Figure 4: Module imprint lengths at each operating speed obtained from numerical simulations. (Red cross indicates the average of the module imprint lengths.)

Based on the numerical results, it is concluded that the operating speed influences the energy imparted to the ground and the behaviour of the RDC module. The effect of operating speed on the performance of RDC also depends on the site conditions. Based on the results of module imprint lengths in Figure 4, an operating speed range between 10 to 14 km/h is recommended. However, this suggested operating speed range needs to be further verified by field trials, since the operating speed also causes wear-and-tear on the mechanical components and discomfort for operator. As reported by Avalle et al. (2009), speeds above 12 km/h may result in an uncomfortable ride for the operator and may induce damage to the module frame. In addition, there are some sites that contain several small working areas and, in such situations, the operating speed of the roller is difficult to be maintained within the typical range (Scott et al., 2020). In general, conducting a field trial is encouraged prior to the actual tests to examine whether the recommended operating speed range can be achieved and used at each particular site.

5 GROUND CONDITIONS

5.1 RELATIONSHIPS BETWEEN THE MICROSCOPIC PARAMETERS AND MACROSCOPIC PROPERTIES OF SOIL

As mentioned above, the linear contact model was adopted to describe the interaction between the particles in the numerical model. Five input parameters are required in the linear contact model, namely normal and shear stiffnesses, normal and shear damping ratios and the coefficient of friction. According to Chen et al. (2021), for quartzose materials, the ratio between the normal and shear stiffnesses is unity and the damping ratios are 0.1. Therefore, the numerical macroscopic behaviours of the soil particles are mainly affected by the contact stiffness (normal and shear stiffnesses) and the coefficient of friction, if the initial porosity and particle size remain constant.

The relationships between DEM input parameters (contact stiffness and coefficient of friction) and soil macroscopic behaviour are obtained by conducting several numerical triaxial tests, with one input parameter being changed in-turn, while the others remain constant. As mentioned above, the soil used in this study is the same as that adopted by Chen et al. (2021), therefore, similar to Chen et al. (2021), the numerical particles used in numerical triaxial tests were generated with diameters between 1 and 3 mm. The triaxial test sample had a diameter of 50 mm and a height of 100 mm. Similar to the experimental triaxial tests, the numerical triaxial simulations incorporated three stages. Firstly, the DEM particles were generated randomly to fill an enclosed cylinder and

then fell under gravity from a constant height. The top loading cap moved up and down to compact particles to help them settle and to match the experimental porosity. After all particles reached a static and steady state, the target confining pressure was then applied during the second stage. In the third stage, the axial strain was increased by displacing the top plate vertically at a constant velocity (10 mm/s in this study), and the confining pressure was maintained at the same time. The loading velocity was set as 1 mm/min in the physical triaxial tests. However, due to the computational and time constraints, the samples were sheared at a higher loading velocity in the numerical model. Numerical triaxial tests were conducted with different loading velocities to investigate the effects of loading velocity on test results. It was found that the loading velocity of 10 mm/s provided a computationally efficient model without compromising the accuracy of the results. A similar procedure of selecting the loading velocity in the numerical triaxial tests has been adopted in many studies, such as Gu et al. (2017), Kozicki et al. (2014), and Mahabadi et al. (2010).

In order to investigate the effects of contact stiffness on the macroscopic behaviour of the soil, several numerical triaxial simulations were conducted at a confining pressure of 250 kPa with a contact stiffness varied from 450 to 1050 kN/m, while maintaining the coefficient of friction constant at 0.25 in all simulations. In general, it can be seen from Figure 5 that the value of the contact stiffness has a significant influence on the slope of the stress-strain curves. The peak deviatoric stress is less affected by the contact stiffness. The influence of the contact stiffness on the slope of the stress-strain curves shows a decreasing trend when the value of contact stiffness increases to a certain value. In other words, the contraction of sample during the triaxial tests is affected by the variation of contact stiffness. As the contact stiffness increases, the value and the duration of the compression of the sample gradually reduces, whereas the contact stiffness has less influence on the dilatancy of the sample. The same phenomenon was observed by Plassiard et al. (2009), Gabrieli et al. (2009), Tapias et al. (2011) and Marczewska et al. (2016). They performed a series of numerical DEM triaxial tests and reported that, the initial slope of the stress-strain curves increases with the increasing contact stiffness values for lower values of contact stiffness. In terms of higher contact stiffness values, the effect of contact stiffness on the initial slope of the stress-strain curves is very small.

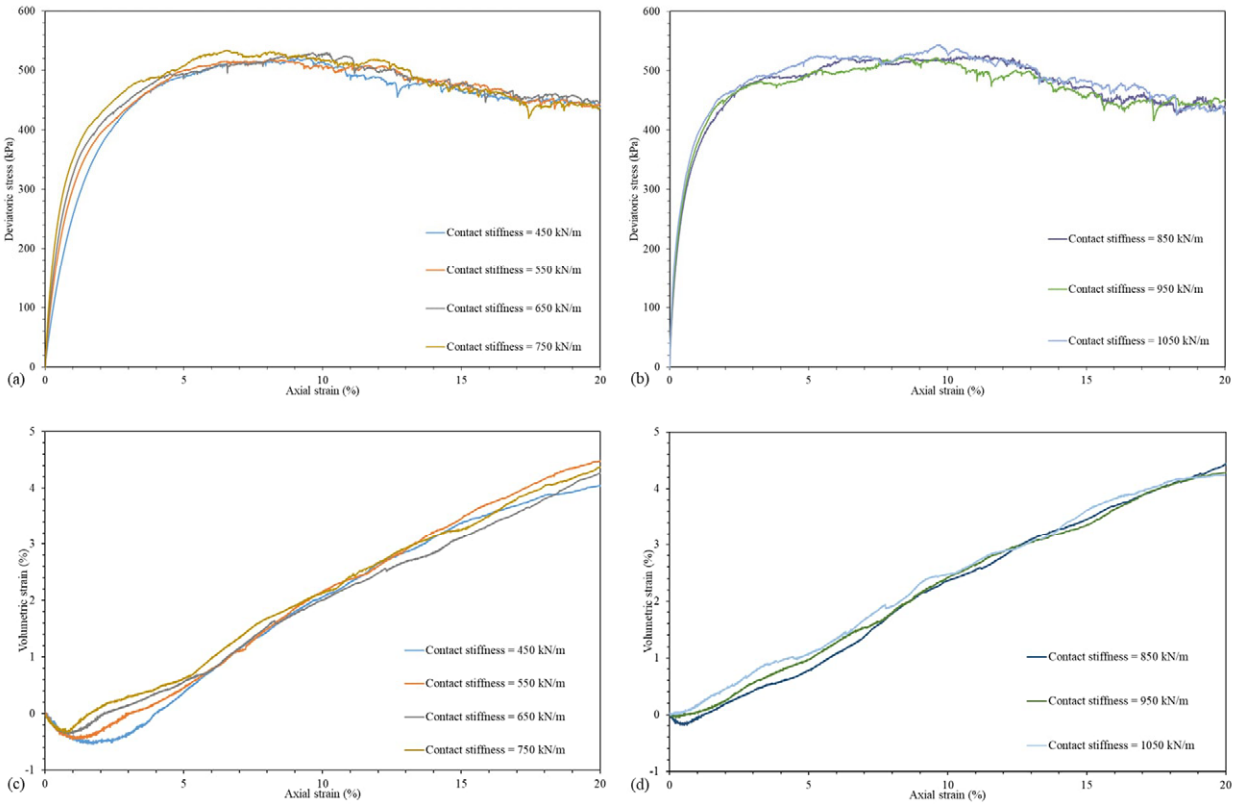

Figure 5: Triaxial tests at a confining pressure of 250 kPa with different contact stiffness values: (a) and (b) stress-strain curves; (c) and (d) volumetric curves.

According to Plassiard et al. (2009) and Wang and Li (2014), the initial Young's modulus (E), Poisson's ratio (v) and the internal angle of friction (φ) can be determined from the stress-strain curves, as shown in Figure 6. The effect of Poisson's ratio on the soil macroscopic behaviour is not investigated in this study, since Poisson's ratio is the ratio between the soil's lateral and longitudinal strains and it mainly relates to soil deformation behaviour. In this study, the soil particles are placed in a chamber and the horizontal deformation of the soil is constrained by the chamber. Therefore, the effect of Poisson's ratio is difficult to investigate.

Based on Figure 6, it can be seen from Figure 5 that the soil's initial Young's modulus increases with rising contact stiffness and the peak stress value is not affected by the variation of contact stiffness. In this study, the effect of contact stiffness on the initial Young's modulus is examined since the soil's stiffness is directly related to soil displacement and the performance of the impact roller. Figure 7 shows the relationship between the DEM input contact stiffness value and the soil's initial Young's modulus, and an almost linear relationship is observed. Therefore, the maximum and minimum values of contact stiffness (1050 and 450 kN/m), which correspond to a soil's initial Young's modulus of approximately 69 and 25 MPa, respectively, are adopted in the numerical RDC simulations that follow.

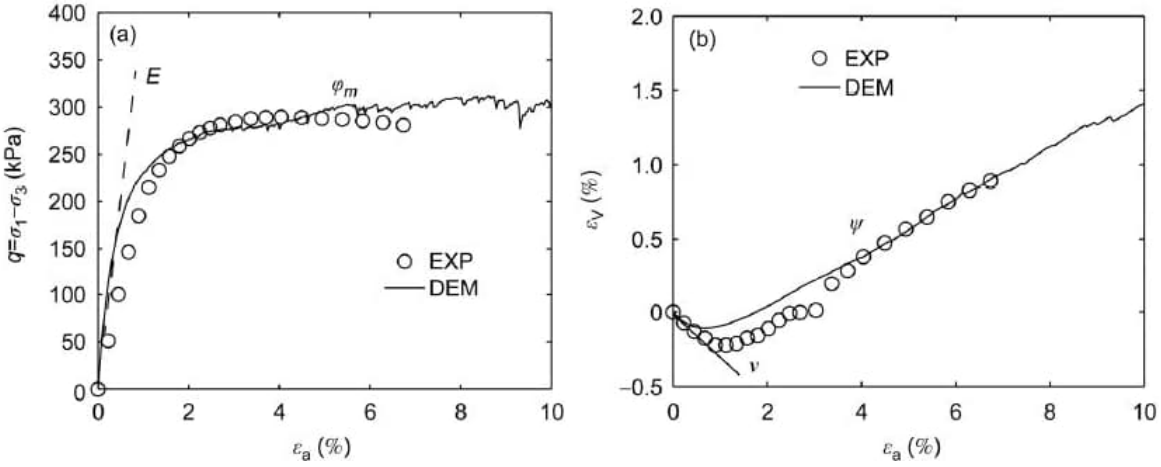

Figure 6: Soil properties obtained from triaxial tests (Wang and Li, 2014).

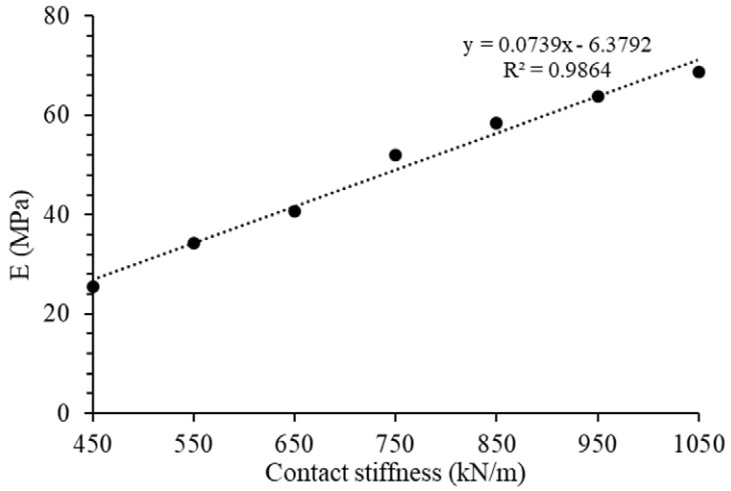

Figure 7: The effect of contact stiffness on the soil's initial Young's modulus.

A similar process was performed to investigate the effect of the coefficient of friction on the macroscopic stress-strain behaviour of the soil. A series of numerical triaxial simulations were conducted at a confining pressure of 250 kPa with a coefficient of friction varying from 0.23 to 0.27, while the contact stiffness was maintained

constant at 650 kN/m. The results of the numerical triaxial simulation with various coefficients of friction are shown in Figure 8. It can be seen that the soil's elastic response is not affected by the variation in the coefficient of friction. The values of peak stress and soil dilatancy response increase with rising coefficient of friction. In terms of the soil's macroscopic parameters, the coefficient of friction has a negligible effect on the initial Young's modulus and Poisson's ratio. The internal angle of friction and the dilatancy angle show an increasing trend as the coefficient of friction increases. These are consistent with the findings from Coetzee and Els (2009), Gabrieli et al. (2009), Kozicki and Tejchman (2009) and Wang and Li (2014). They stated that the increase in coefficient of friction results in the internal angle of friction increasing, while the soil elastic response is not affected by changes in the coefficient of friction.

In order to obtain the Mohr-Coulomb failure envelope to evaluate the soil internal angle of friction, numerical triaxial simulations were conducted at a confining pressure of 150 kPa in the same manner as those performed at the 250 kPa confining pressure. Figure 9 illustrates the relationship between the microscopic coefficient of friction and the soil's macroscopic internal angle of friction. From Figure 9, it is clear that the coefficient of friction and soil internal angle of friction have an almost linear relationship with each other. Again, the maximum and minimum microscopic coefficient of friction (0.27 and 0.23), which correspond to macroscopic internal angles of friction of 28° and 20°, respectively, are used to conduct the numerical RDC simulations that follow.

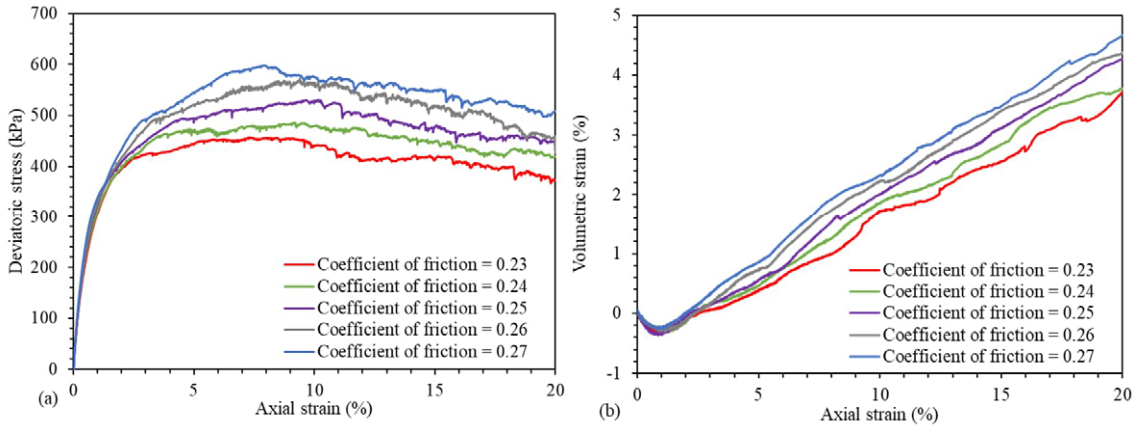

Figure 8: Triaxial tests at a confining pressure of 250 kPa with different coefficient of friction values: (a) stress-strain curves; (b) volumetric curves.

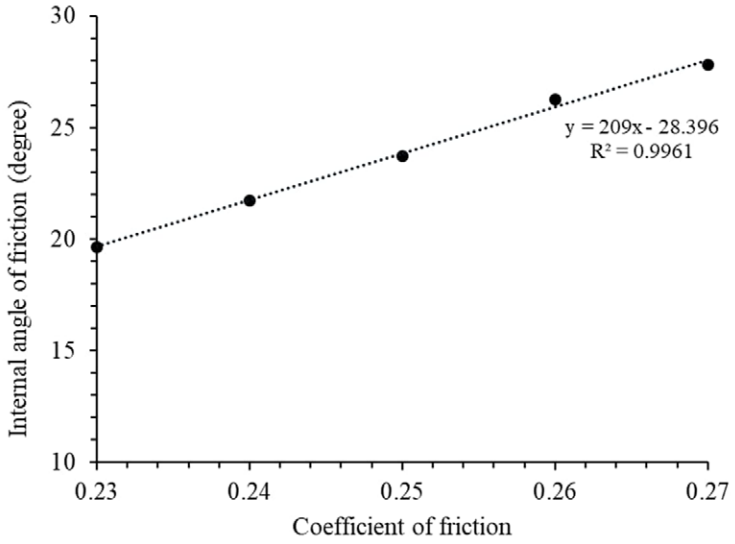

Figure 9: The effect of coefficient of friction on soil internal angle of friction.

Table 5 presents the matrix of numerical RDC simulations with different ground conditions. In this case, all numerical RDC simulations were conducted at an operating speed of 256 mm/s, which corresponds to a prototype speed of 12 km/h. In total, eight simulations were performed for the 3.64 and 5.46 kg scaled modules at two different normal contact stiffnesses and two different coefficients of friction, with each simulation being carried out up to 10 module passes.

Table 5: Simulation matrix for various ground conditions.

Simulation no.	Scale module mass (kg)	DEM microscopic normal contact stiffness (kN/m)	Soil macroscopic initial Young's modulus (MPa)	DEM microscopic coefficient of friction	Soil macroscopic internal angle of friction
9	3.64	450	25	0.25	24°
10	3.64	1050	69	0.25	24°
11	5.46	450	25	0.25	24°
12	5.46	1050	69	0.25	24°
13	3.64	650	52	0.23	20°
14	3.64	650	52	0.27	28°
15	5.46	650	52	0.23	20°
16	5.46	650	52	0.27	28°

5.2 EFFECTS OF INITIAL YOUNG'S MODULUS AND INTERNAL ANGLE OF FRICTION ON SOIL DENSIFICATION

Plots of soil displacements after ten module passes and the pressures induced by the module at 55 mm depth below the ground obtained from Simulations 9–12 are shown in Figures 10 and 11. The boxplot in Figure 11 was plotted based on the obtained pressures in ten module passes. The top and bottom of the box are the 75 and 25% quartile values, respectively, and the line drawn inside the box is the median value of the measured pressures. The top and bottom whiskers represent the maximum and minimum pressures, respectively. The red cross is the average pressure calculated from the obtained pressure results. It can be seen that a higher soil's initial Young's modulus results in smaller soil displacements, as one would expect, and increased pressures for both the 3.64 and 5.46 kg modules. In addition, as the soil's initial Young's modulus increases, the soil becomes stiffer and pressure waves are able to be more readily propagated through the soil body, which then results in greater pressure values. Comparing soil displacements and induced pressure values obtained from Simulations 9 and 10, with those obtained from Simulations 11 and 12, it is clear that, the heavier module produces greater displacements and higher pressures, which is consistent with the conclusion drawn earlier in the paper.

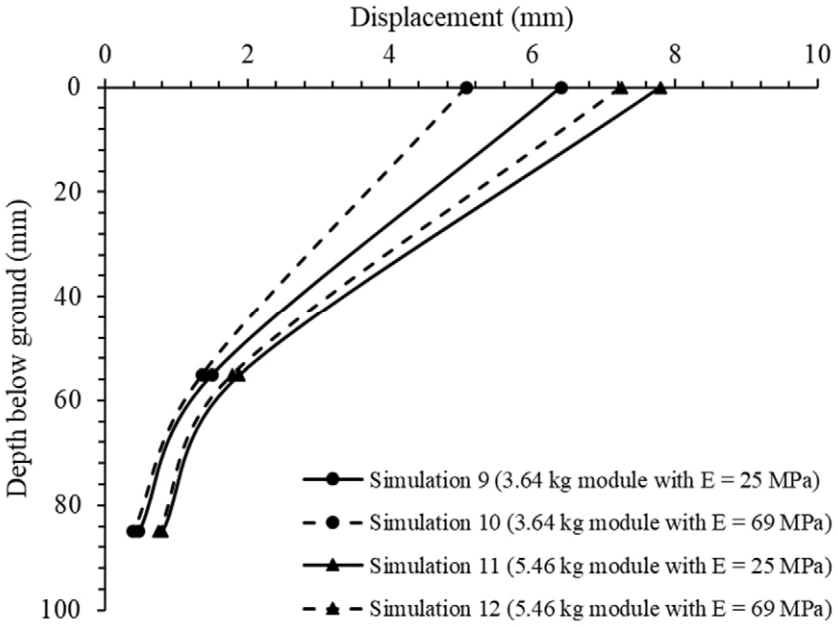

Figure 10: The effect of soil initial Young's modulus on soil displacements after 10 module passes.

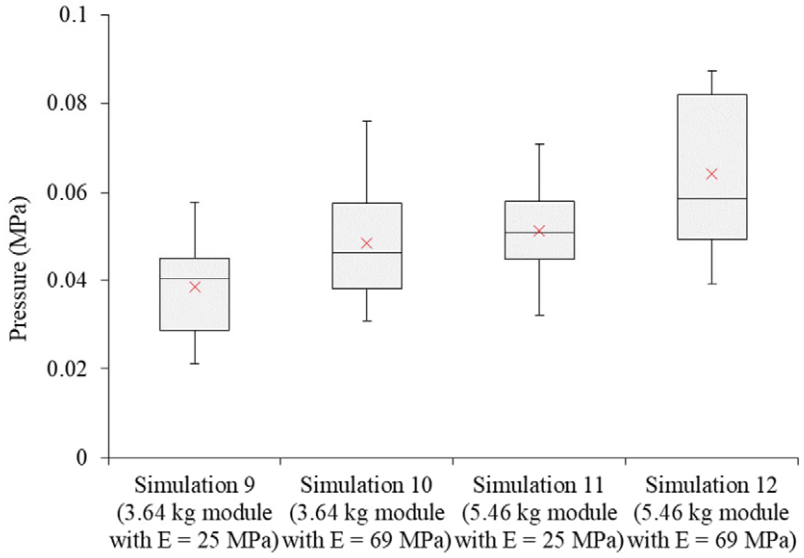

Figure 11: The effect of soil initial Young's modulus on the induced pressures at 55 mm depth below the ground.

A similar phenomenon is observed with respect to soil displacements after 10 module passes and pressures at 55 mm depth below the ground from Simulations 13–16, as shown in Figures 12 and 13. A reduced internal angle of friction results in increased soil displacements and lower pressure values. This is expected, as lower values of internal angle of friction are associated with less dense soil.

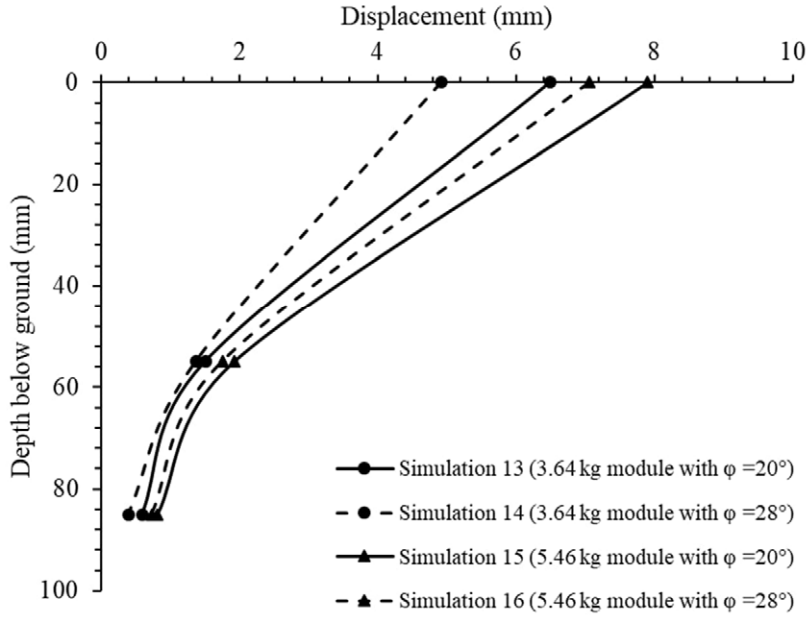

Figure 12: The effect of soil internal angle of friction on soil displacements after 10 module passes.

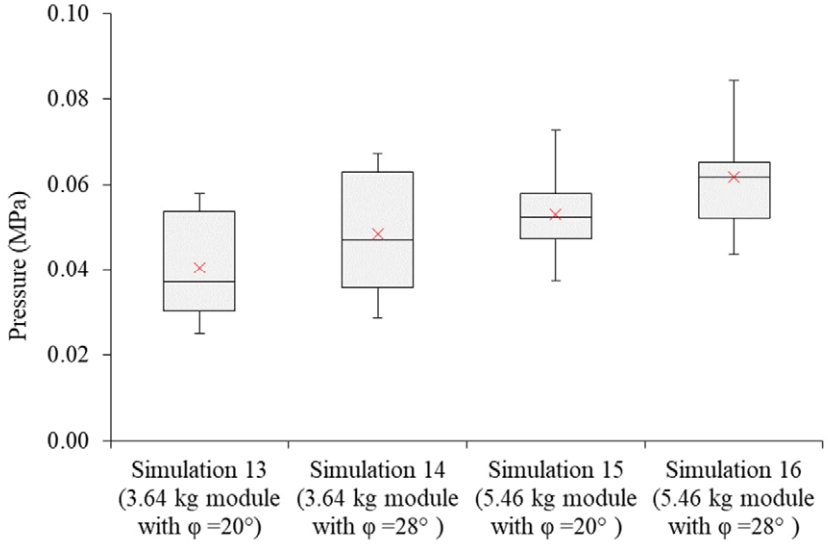

Figure 13: The effect of soil internal angle of friction on the induced pressures at 55 mm depth below the ground.

In general, based on the results from Simulations 9 to 16, shown in Figures 10 to 13, it is evidenced that different soil properties (soil initial Young's modulus and internal angle of friction) can affect the soil response due to the impact roller compaction. A greater soil initial Young's modulus and a higher internal angle of friction decrease soil displacements and increase pressures. In addition, these results further confirm the conclusion that the greater module weight imparts a greater amount of energy to the ground and produces greater soil displacements. It is also worth mentioning that all of the conclusions drawn from this study are based on a limited number of roller passes and a relatively narrow range of soil initial Young's moduli and internal angles of friction. An extensive parametric study on each parameter is encouraged, however, due to time and computational constraints, only a limited number of numerical RDC simulations could be conducted. For reference purposes, one RDC simulation, consisting of 25 passes and approximately 54,000 particles, typically took approximately 30 days to run on the aforementioned supercomputer. Although a limited number of numerical parametric studies have been conducted, the obtained relationships between the microscopic DEM input parameters and the macroscopic soil behaviour

are in good agreement with those reported by previous researchers (e.g. Plassiard et al., 2009; Gabrieli et al., 2009; Tapias et al., 2011; Wang and Li, 2014; Marczewska et al., 2016). The results obtained from Simulations 9–16 provide guidance on the performance of RDC in different ground conditions. However, extrapolating data and drawing conclusions beyond the range of these simulations should be treated with caution. Based on the obtained results, it is suggested that the roller is less able to significantly improve stiff soil or soil with greater initial shear strength.

6 SUMMARY AND CONCLUSIONS

This paper has examined the effects of module weight, operating speed and different ground conditions on the effectiveness of the 4-sided impact roller using a developed numerical FEM-DEM model. Results of the numerical model were assessed from four aspects, namely the energy imparted to the ground, soil velocity vectors, module imprint lengths and soil displacements at different depths. It was found that the heavier module produces greater ground improvement results in terms of a greater energy delivered to the soil per impact and larger induced soil displacements. The operating speed influences the amount of energy and the manner by which the energy is delivered to the ground. The imparted energy increases with operating speed. The roller module tends to skip on the ground at high operating speeds and in this case, the energy is delivered by the corners rather than the faces of the module. A greater soil initial Young's modulus and a higher internal angle of friction decrease soil displacements and increase pressure readings induced by the roller.

Overall, this study facilitates improved understanding of the factors that affect the effectiveness and application of RDC. It is important to note that, as this numerical model relies heavily on supercomputing facilities, it remains a research, rather than a practical, tool. In addition, the effects of different designs (3- and 5-sided modules) on ground improvement results will be investigated in future work.

7 ACKNOWLEDGEMENTS

The authors wish to acknowledge the computational resources provided by the Phoenix HPC service at the University of Adelaide.

8 FUNDING

This research did not receive any specific grant from funding agencies in the public, commercial, or not-for-profit sectors.

9 CONFLICT OF INTEREST

The authors declare that they have no conflict of interest.

10 REFERENCES

Altaee, A., Fellenius, B. H. 1994. Physical modeling in sand. *Canadian Geotechnical Journal,* 31**,** 420-431.

Avalle, D., Carter, J. 2005. Evaluating the improvement from impact rolling on sand. *Proc. 6th Int. Conf. on Ground Improvement Techniques*, Coimbra, Portugal, 8pp.

Avalle, D. L., McKenzie, R. W. 2005. Ground improvement of landfill site using the square impact roller. Australian Geomechanics, 40, 15-21.

Avalle, D. L, Scott, B. T, Jaksa, M. B. 2009. Ground energy and impact of rolling dynamic compaction e results from research test site. *In: Proceedings of the 17th International Conference on Soil Mechanics and Geotechnical Engineering*, Vol. 3, Alexandria, Egypt, p. 2228-31.

Bouazza, A., Avalle, D. L. 2006. Effectiveness of rolling dynamic compaction on an old waste tip. *ISSMGE 5th International Congress on Environmental Geotechnics*, Cardiff, 1.

Bradley, A. C., Jaksa, M. B., Kuo, Y.-L. 2019. Examining the kinematics and energy of the four-sided impact roller. *Proceedings of the Institution of Civil Engineers - Ground Improvement,* 172**,** 297-304.

Calvetti, F., Di Prisco, C., Nova, R. 2004. Experimental and numerical analysis of soil–pipe interaction. *Journal of geotechnical and geoenvironmental engineering,* 130**,** 1292-1299.

Calvetti, F., Viggiani, G., Tamagnini, C. 2003. A numerical investigation of the incremental behavior of granular soils. *Rivista italiana di geotecnica,* 37**,** 11-29.

Chen, Y., Jaksa, M., Kuo, Y., Scott, B. 2021. Discrete element modelling of the 4-sided impact roller. *Computers and Geotechnics* Available from https://doi.org/10.1016/j.compgeo.2021.104250.

Clifford, J.M. 1980. The development and use of impact rollers in the construction of earthworks in southern Africa. *CSIR Report 373. Pretoria, South Africa: National Institute for Transport and Road Research.*

Coetzee, C., Els, D. 2009. Calibration of granular material parameters for DEM modelling and numerical verification by blade–granular material interaction. *Journal of Terramechanics,* 46**,** 15-26.

Gabrieli, F., Cola, S., Calvetti, F. 2009. Use of an up-scaled DEM model for analysing the behaviour of a shallow foundation on a model slope. *Geomechanics and Geoengineering: An International Journal,* 4**,** 109-122.

Gu, M., Han, J. & Zhao, M. 2017. Three-dimensional discrete-element method analysis of stresses and deformations of a single geogrid-encased stone column. *International Journal of Geomechanics*, 17, 04017070.

Jaksa, M. B., Airey, D. W., Scott, B. T., Kuo, Y. L., Ranasinghe, R. A. T. M., Bradley, A. C., Chung, O. Y., Li, Y., Chen, Y. 2019. Quantifying the Effect of Rolling Dynamic Compaction. *Proceedings of the 4th World Congress on Civil, Structural, and Environmental Engineering.* Rome, Italy.

Jaksa, M. B., Scott, B. T., Mentha, N., Symons, A., Pointon, S., Wrightson, P., Syamsuddin, E. 2012. Quantifying the zone of influence of the impact roller. *ISSMGE-TC 211 International Symposium on Ground Improvement IS-GI Brussels*.

Kim, K. 2011. *Impact Rollers (Soil Compaction) Numerical Simulation of Impact Rollers for Estimating the Influence Depth of Soil Compaction* (1st ed.). Saarbrucken: LAP LAMBERT Academic Publishing GmbH & Co. KG.

Kozicki, J., Tejchman, J. 2009. Numerical simulations of triaxial test with sand using DEM. *Archives of Hydro-Engineering and Environmental Mechanics,* 56**,** 149-172.

Kozicki, J., Tejchman, J. & Mühlhaus, H. B. 2014. Discrete simulations of a triaxial compression test for sand by DEM. *International Journal for Numerical and Analytical Methods in Geomechanics*, 38, 1923-1952.

Kuo, Y., Jaksa, M., Scott, B., Bradley, A., Power, C., Crisp, A., Jiang, J. 2013. Assessing the effectiveness of rolling dynamic compaction. *Proceedings of the 18th International Conference on Soil Mechanics and Geotechnical Engineering*, Paris.

Li, Y., Airey, D., Jaksa, M. 2020. Evaluating the effective depth of rolling dynamic compaction with a three-sided compactor. *International Journal of Physical Modelling in Geotechnics,* 0**,** 1-15.

LSTC. 2018. LS-DYNA Keyword User's Manual. Livermore, California: Livermore Software Technology Corporation, ISBN: 0-9778540-2-7.

Mahabadi, O., Lisjak, A., Grasselli, G., Lukas, T. & Munjiza, A. Numerical modelling of a triaxial test of homogeneous rocks using the combined finite-discrete element method. *Proc. European Rock Mechanics Symp.(EUROCK2010)*, Lausanne, Switzerland, 2010. 173-176.

Marczewska, I., Rojek, J., Kačianauskas, R. 2016. Investigation of the effective elastic parameters in the discrete element model of granular material by the triaxial compression test. *Archives of Civil and Mechanical Engineering,* 16**,** 64-75.

Plassiard, J.-P., Belheine, N., Donzé, F.-V. 2009. A spherical discrete element model: calibration procedure and incremental response. *Granular Matter,* 11**,** 293-306.

Scott, B., Jaksa, M. 2008. Quantifying the influence of rolling dynamic compaction. *Proc. 8YGPC***,** 199-204.

Scott, B., Jaksa, M. 2014. Evaluating rolling dynamic compaction of fill using CPT. *Proceedings of the 3rd International Symposium on Cone Penetration Testing*. 941-948.

Scott, B., Jaksa, M., Mitchell, P. 2019. Depth of influence of rolling dynamic compaction. *Proceedings of the Institution of Civil Engineers-Ground Improvement***,** 1-10.

Scott, B., Jaksa, M., Syamsuddin, E. 2016. Verification of an impact rolling compaction trial using various in situ testing methods. *Proc. of 5th Int. Conf. on Geotechnical and Geophysical Site Characterisation.*

Scott, B. T., Jaksa, M. B., Mitchell, P. W. 2020. Influence of towing speed on effectiveness of rolling dynamic compaction. *Journal of Rock Mechanics and Geotechnical Engineering,* 12**,** 126-134.

Tapias, M. A., Alonso Pérez De Agreda, E., Gili Ripoll, J. A. 2011. Analysis of micro-properties for triaxial behaviour on coarse aggregates using DEM. *PARTICLES II: Proceedings of the II International Conference on Particle-Based Methods: fundamentals and applications*, CIMNE, 550-561.

Wang, X., Li, J. 2014. Simulation of triaxial response of granular materials by modified DEM. *Science China Physics, Mechanics & Astronomy,* 57**,** 2297-2308.